



PCCP

The reducibility and oxidation states of oxide-supported rhenium: Experimental and theoretical investigations

Journal:	<i>Physical Chemistry Chemical Physics</i>
Manuscript ID	CP-ART-10-2022-004784.R1
Article Type:	Paper
Date Submitted by the Author:	09-Nov-2022
Complete List of Authors:	Ting, Kah Wei; Hokkaido university, Catalysis Research Center Mine, Shinya; Hokkaido University, Catalysis; Osaka Prefecture University, Applied Chemistry, Graduate School of Engineering Ait El Fakir, Abdellah; Hokkaido university, Institute for Catalysis Du, Pengfei; Hokkaido university, Institute for Catalysis Li, Lingcong; Hokkaido University, Institute for Catalysis Siddiki, S.; Hokkaido University, Catalysis Toyao, Takashi; Hokkaido university, Institute for Catalysis Shimizu, Ken-ichi; Hokkaido University, Catalysis Research Center

SCHOLARONE™
Manuscripts

The reducibility and oxidation states of oxide-supported rhenium: Experimental and theoretical investigations

Kah Wei Ting,^a Shinya Mine,^a Abdellah Ait El Fakir,^a Pengfei Du,^a Lingcong Li,^a S. M. A. Hakim Siddiki,^b Takashi Toyao,^{*a} Ken-ichi Shimizu^{*a}

^a Institute for Catalysis, Hokkaido University, N-21, W-10, Sapporo, Hokkaido 001-0021, Japan

^b Department of Chemistry, Tokyo Metropolitan University, 1-1 Minami Osawa, Hachioji, Tokyo 192-0397, Japan

*Corresponding authors

Takashi Toyao, Ken-ichi Shimizu

E-mail: toyao@cat.hokudai.ac.jp, kshimizu@cat.hokudai.ac.jp

Abstract

The activity and stability of supported metal catalysts, which exhibit high efficiency and activity, are significantly influenced by the interactions between the metal and the support, that is, metal–support interactions (MSIs). Here, we report an investigation of the MSIs between supported rhenium (Re) and oxide supports such as TiO₂, SiO₂, Al₂O₃, MgO, V₂O₅, and ZrO₂ using experimental and computational approaches. The reducibility of the Re species was found to strongly depend on the oxide support. Experimental studies including temperature-programmed reduction by H₂ as well as Re L₃- and L₁-edge X-ray absorption near edge structure (XANES) analysis revealed that the valency of the Re species started to decrease upon H₂ reduction in the 200–400 °C range, except for Re on MgO, where the shift occurred at temperatures above 500 °C. The dependence of the Re L₃- and L₁-edge XANES spectra of the oxide-supported Re catalysts on the size of Re was also examined.

1. Introduction

Supported metals are efficient catalysts^{1,2} whose activity and stability can be significantly influenced by metal–support interactions (MSIs),^{3–5} which can alter the characteristics of the metals, their interfaces, and perimeter sites.^{6–8} The nature of the active sites created in these environments can be affected by the size, shape, and dispersion of the metal species.^{9–11} MSIs also affect the resistance of metals to sintering, which often leads to deactivation of the catalysts.^{12–15} Therefore, understanding the MSIs in oxide-supported metal catalysts by clarifying their behavior with respect to the type of metal and oxide is essential for tailoring their activity, stability, and selectivity.

Among the various supported metal catalysts, supported rhenium (Re) catalysts show remarkable technological potential in heterogeneous catalysis.^{16–25} In particular, supported Re catalysts promote several valuable reductive catalytic processes,^{26–31} including the hydrogenation of carboxylic acid derivatives^{32–36} and CO₂.^{37–43} However, although previous studies have stimulated the development of highly active and selective catalysts for these processes, the precise nature of the catalytically active Re species has not been elucidated, despite them having been the subject of scientific investigations for years.^{44–53} This is primarily because Re, which is often highly dispersed on supports, is difficult to reduce and can exist in several oxidation states.^{54–63} To address this deficit, comprehensive studies on supported Re catalysts must be conducted to gain fundamental insight into the behavior of catalytically active Re species.

Systematic experimental and computational studies were previously conducted by our group to investigate the MSIs between supported Re and various oxide supports.⁶⁴ The degree of dispersion and aggregation of the supported Re metal on oxide supports were found to be correlated with their electronic properties, namely the position of the conduction band minimum [CBM, that is, electron affinity (EA)] of the oxide support and the Fermi energy [E_F , that is, work function (WF)] of Re. Metal oxides with an EA higher than the WF of Re, such as TiO₂, V₂O₅, and CeO₂, can accept electrons from Re to their CBs, inducing strong MSIs (high E_{ads} of Re) that lead to a high degree of dispersion of the supported Re. In contrast, metal oxides with an EA lower than the WF of Re, such as MgO and Al₂O₃, cannot accept electrons from Re to their CBs, thereby inducing weak MSIs (low E_{ads} of Re) that lead to a low degree of dispersion of the supported Re. Although the degree of dispersion and aggregation of the supported Re on various oxide supports have been investigated, the oxidation states of the supported Re are largely unknown. This necessitates comprehensive studies on the oxidation states of supported Re.

Therefore, a systematic investigation was conducted in this study to characterize the reducibility and oxidation states of 5 wt.% Re supported on various oxide supports, including TiO₂, SiO₂, Al₂O₃, MgO, V₂O₅, and ZrO₂. Temperature-programmed reduction by H₂ (H₂-TPR) as well as Re L₃- and L₁-edge X-ray absorption near edge structure (XANES) measurements were conducted, which indicated that the reducibility of Re species strongly depended on the oxide support. Additionally, XANES simulations were performed using the Finite difference method near edge structure (FDMNES) software,^{65,66} which revealed the structural dependence of the Re L₃- and L₁-edge XANES spectra.

2. Methods

Materials and sample preparation

TiO₂ (ST-01, 188 m² g⁻¹) and SiO₂ (CARiACT Q-10, 300 m² g⁻¹) were purchased from Ishihara Sangyo and Fuji Silysia Chemicals, respectively. Al₂O₃ (74 m² g⁻¹) was prepared by calcining boehmite (Catapal B Alumina, Sasol) for 3 h at 900 °C. MgO (JRC-MGO-3-500A, 24 m² g⁻¹) and ZrO₂ (JRC-ZRO-5, 194 m² g⁻¹) were provided by the Catalysis Society of Japan, whereas V₂O₅ (3 m² g⁻¹) was purchased from Sigma-Aldrich. The specific surface area (SSA) for each support as provided by the supplier is shown in parentheses, except for the SSA of V₂O₅ which is measured in-house via N₂ adsorption. Re₂O₇ (≥ 99%) and ReO₂ (≥ 99%) were purchased from Strem Chemicals Inc. and HydruS Chemical Inc., respectively. ReO₃ (≥ 99%) was obtained from Alfa Aesar. NH₄ReO₄ (≥ 99%) and Re powder (≥ 99%, mesh = 100 μm) were purchased from Sigma Aldrich. All reagents and materials were used as received without further purification. He (≥ 99.995%), H₂ (≥ 99.99%) and other gas mixture such as 10% CO/He and 5% H₂/Ar were obtained from Air Water Inc.

Re/support catalysts with 5 wt.% Re [denoted as Re(5)/support] were prepared using a simple impregnation method by mixing the support material with an aqueous solution of NH₄ReO₄ (Sigma-Aldrich). Briefly, NH₄ReO₄ (0.36 g) was added to a glass vessel (500 mL) containing deionized water (400 mL). After completely dissolving the NH₄ReO₄ by stirring, the support material (4.75 g) was added to the solution, followed by stirring at 200 rpm for 30 min at 20 °C. Subsequently, water was removed from the reaction mixture via evaporation *in vacuo*, followed by drying at 110 °C for 12 h. The resulting powder was calcined for 3 h at 500 °C in air, except for Re(5)/V₂O₅, which was not calcined to prevent sublimation of the Re species. The final sample was obtained by reduction under flowing H₂ (20 mL min⁻¹) for 0.5 h.

Characterization

Scanning transmission electron microscopy (STEM) analysis was conducted using JEM-ARM200F and FEI Titan G2 electron microscopes. The samples were pre-treated under flowing H₂ (20 mL min⁻¹) at 500 °C for 0.5 h prior to STEM analysis, and were exposed to air during analysis due to the apparatus setup. H₂-TPR was performed using BELCAT II equipment (MicrotracBEL Corp., Japan). 40 mg of each sample were heated to 900 °C with a heating rate of 10 °C min⁻¹ under 40 mL min⁻¹ flow of 5% H₂/Ar.

FT-IR spectra for CO adsorption were measured on JASCO FT/IR-4200 equipped with a mercury-cadmium-telluride (MCT) detector. Each sample (40 mg) were pressed into self-supporting disks (φ = 20 mm) which was then placed in a quartz FT-IR cell with CaF₂ windows connected to a gas flow setup. Each sample was pre-treated at 500 °C for 0.5 h under a flow of 10% H₂/He (100 mL min⁻¹), and then cooled to 50 °C under He flow. After sufficient cooling, 1% CO/He (100 mL min⁻¹) was introduced to the cell for at least 5 min and purged with He subsequently. Spectra were collected by accumulating 20 scans (resolution: 4 cm⁻¹). Background spectrum was collected at 50 °C under He atmosphere.

Re L₃- and L₁-edge XANES spectra were recorded in transmittance mode at the BL14B2 beamline of SPring-8 (proposals 2020A1695 and 2021A1615) using a Si (311) double-crystal monochromator. The samples were pressed into self-supporting pellets (φ = 10 mm) and introduced into a quartz cell equipped with Kapton film windows and gas lines with a dead volume of approximately 20 mL.⁶⁷ Pelletized samples

were heated under a flow of 5% H₂/He (100 mL min⁻¹) at temperatures up to 700 °C with a heating rate of 10 °C min⁻¹. Data analysis was performed using the Athena software ver. 0.9.25, which is included in the Demeter package.⁶⁸ Linear combination fitting (LCF) was performed over a fitting range of -20 to 30 eV relative to the absorption edge (E₀) using Re powder (Re⁰), ReO₂ (Re⁴⁺), ReO₃ (Re⁶⁺), and NH₄ReO₄ (Re⁷⁺) as standards.

Computational methods

All calculations were performed based on the spin-polarized density functional theory (DFT) using the Vienna *ab initio* simulation package (VASP.5.4.4).^{69,70} The revised Perdew–Burke–Ernzerhof functional for solids (PBEsol)⁷¹ was employed in combination with the projector-augmented wave (PAW) method.⁷² A kinetic energy cutoff of 400 eV was set for the plane-wave basis sets. Gaussian smearing with a width of 0.2 eV was applied for the occupation of the electronic levels. The Brillouin zone was sampled using 2 × 2 × 1 Monkhorst–Pack grids. Van der Waals interactions were described using the dispersion-corrected DFT-D3 method (Becke–Johnson).⁷³ The convergence of force on each atom was set to 0.03 eV Å⁻¹.

The surface of anatase TiO₂ (101) was simulated using a four-layer supercell slab model (**Figure 1 and S1**). Re clusters of 1, 3, 13, and 20 atoms were placed on TiO₂ (101); these configurations are denoted as Re₁/TiO₂, Re₃/TiO₂, Re₁₃/TiO₂, and Re₂₀/TiO₂, respectively. A 2 × 2 slab model (Ti₄₈O₉₆) was used for Re₁/TiO₂, Re₃/TiO₂, and Re₁₃/TiO₂, whereas a 2 × 4 slab model (Ti₉₆O₁₉₂) was used for Re₂₀/TiO₂ owing to its large cluster size. The repeated slabs along the surface-normal direction were separated by a minimum vacuum-region thickness of 15 Å. The two bottom layers were fixed at their original bulk positions. The effective *U* value (denoted as *U*_{eff}) of *U* – *J* was set to 3 eV in Ti.⁷⁴ The configuration with the most stable total energy after structural relaxation was selected as the model structure.

Re L₁ and L₃-edge XANES spectra were simulated for the DFT-optimized structures of Re₃₆ (0001) slab, Re₁/TiO₂, Re₃/TiO₂, Re₁₃/TiO₂, and Re₂₀/TiO₂ using the FDMNES software.^{65,66} The slab model with 36 Re atoms represented the fully aggregated Re species. The simulated XANES spectra were averaged and normalized based on the number of Re atoms in each supercell. The initial structure of bulk ReO₂ was obtained from the Materials Project⁷⁵ (MP ID:7228) and optimized for atomic positions and cell shape to permit Bader charge analysis.

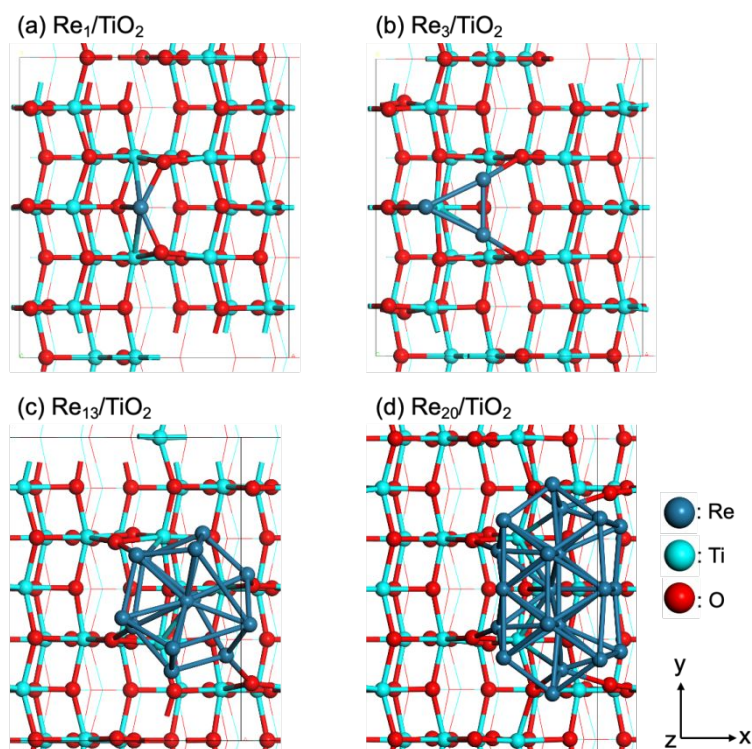


Figure 1. Top-view illustrations of the (a) $\text{Re}_1/\text{TiO}_2(101)$, (b) $\text{Re}_3/\text{TiO}_2(101)$, (c) $\text{Re}_{13}/\text{TiO}_2(101)$, and (d) $\text{Re}_{20}/\text{TiO}_2(101)$ slab models used for DFT calculations.

3. Results and discussion

H_2 -TPR, XANES, and IR studies

The H_2 -TPR profiles of the investigated catalysts are shown in **Figure 2**. The temperature at which the peaks representing H_2 consumption appeared in the profiles increased as follows: $\text{Re}(5)/\text{ZrO}_2 < \text{Re}(5)/\text{TiO}_2 < \text{Re}(5)/\text{SiO}_2 < \text{Re}(5)/\text{Al}_2\text{O}_3 < \text{Re}(5)/\text{MgO}$. All investigated catalysts exhibited one distinct main peak, except $\text{Re}(5)/\text{V}_2\text{O}_5$, which showed several broad, asymmetrical peaks arising from the reduction of Re species, in addition to peaks originating from the reduction of V_2O_5 at approximately 600–700 °C. Overall, the H_2 -TPR profiles shows that for most catalysts, distinct peaks appeared at reduction temperature below 500 °C with no obvious peaks above that temperature, with the exception of $\text{Re}(5)/\text{MgO}$ which has a peak spanning from around 450 °C to 600 °C, and also peaks arising from the reduction of V_2O_5 at around 600 °C.

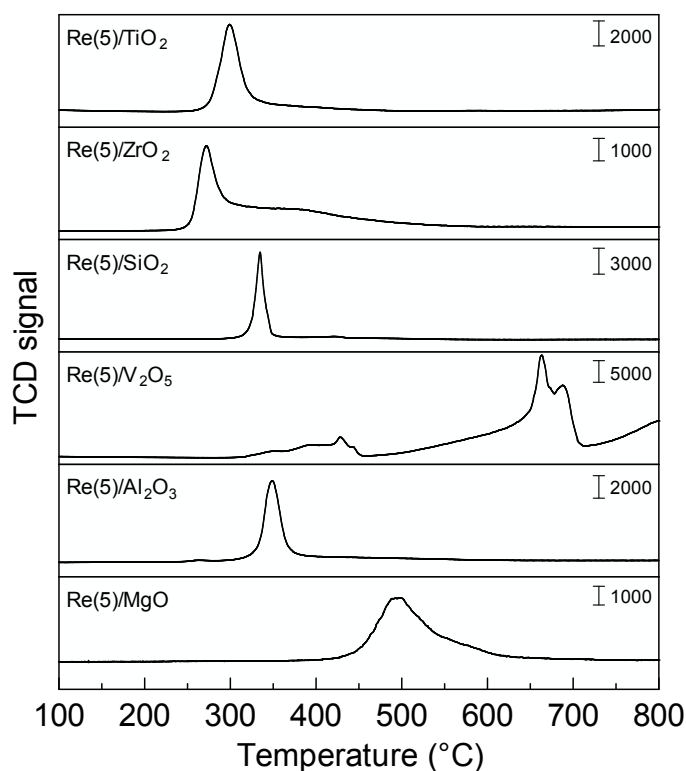


Figure 2. H₂-TPR profiles of Re(5)/support catalysts (support = ZrO₂, TiO₂, SiO₂, V₂O₅, Al₂O₃, and MgO; Re = 5 wt.%). The samples were heated using a temperature ramp rate of 10 °C min⁻¹ under a flow of 5% H₂/Ar (40 mL min⁻¹).

Figure 3A, B show Re L₃-edge XANES spectra of Re(5)/V₂O₅ and Re(5)/MgO, which were recorded under a flow of 5% H₂/He (100 mL min⁻¹) at temperatures between 100 and 700 °C; spectra of reference compounds were recorded at room temperature. A Re metallic powder was also analyzed *ex situ* using a sample that was sealed in a N₂-filled glove bag after the H₂ reduction at 900 °C to prevent the formation of surface ReO_x. The edge positions and shapes of the XANES spectra of the catalysts pretreated with H₂ at temperatures up to 200 °C were consistent with those of the Re₂O₇ reference. This observation indicates that the Re species in these samples existed in highly oxidized states. The intensities of the XANES signals decreased and the edge positions shifted to lower energies following the H₂ reduction at 400 °C. Because the observed variation was a consequence of a change in the energy of the 2p orbital caused by a decrease in the valency of Re,⁴⁸ these results indicate that the valency of Re in all the investigated catalysts began to decrease at ~400 °C. Similar trends have been observed in the XANES spectra of other supported Re samples, such as Re(5)/TiO₂, Re(5)/Al₂O₃, Re(5)/SiO₂, and Re(5)/carbon that were subjected to H₂ reduction at ~300–400 °C, as reported in our previous study.⁷⁶ Note that Re(5)/ZrO₂ was excluded from the aforementioned list because of the contribution of hafnium, an element that is present in almost all Zr oxides, whose L₂-edge absorption (at ~10,739 eV) interferes with the analysis of Re L₃-edge XANES spectra (at ~10,535 eV). The XANES spectra of Re on different supports, including those reported in our previous study,⁷⁶ were compared (**Figure 3C**). High-angle annular dark-field STEM (HAADF-STEM) images are shown in **Figures S2-S7**. The XANES results showed that the edge positions of Re(5)/TiO₂, Re(5)/Al₂O₃, and Re(5)/SiO₂ were nearly identical and lay between those of

the metallic Re and ReO_2 references. However, the edge position and white-line intensity of $\text{Re}(5)/\text{MgO}$ were higher and those of $\text{Re}(5)/\text{V}_2\text{O}_5$ were lower. All the *in situ* XANES spectra showed considerably higher white-line intensities than that of the Re metal powder, suggesting that all the Re species on the oxide supports had valences greater than 0. This is somewhat contrary to the results obtained from the STEM and X-ray diffraction (XRD) measurements as well as the extended X-ray absorption fine structure (EXAFS) analysis, which revealed Re–Re contributions that suggested the formation of metallic Re particles; essentially, all these characterization results indicate the presence of metallic Re clusters/particles to a certain extent, especially in Re/SiO_2 and $\text{Re}/\text{Al}_2\text{O}_3$, which exhibited distinct XRD peaks corresponding to Re. Additionally, although the fraction of oxidized Re species estimated from the XANES spectra did not significantly differ among the studied catalysts, the aforementioned characterization data indicate that the Re dispersion was strongly dependent on the support as indicated in previous studies that the origins of the observed XANES spectra are presumably related to both the valence states and complex structures of Re.^{64,77} Although the effect of various properties of the support including morphologies and defects cannot be ignored, we reported in our previous study⁶⁴ that the effect of the intrinsic properties of each support is more significant on the dispersion of Re species. For instance, we have prepared the low-specific-surface-area rutile TiO_2 (JRC-TIO-5) supported Re sample ($\text{Re}(5)/\text{TiO}_2$ (JRC-TIO-5)). Even though the specific surface area of rutile TiO_2 (JRC-TIO-5) was $3 \text{ m}^2 \text{ g}^{-1}$, which is significantly smaller than that of the anatase TiO_2 (ST-01, $188 \text{ m}^2 \text{ g}^{-1}$) used as the standard support, Re species were present in a highly dispersed and aggregated species >2 nm were not detected.

While the L_3 -edge X-ray absorption white line of transition metals directly reflects the electronic states of the vacant d orbitals of the absorbing atom because it shows $p \rightarrow d$ transitions, the parallel use of L_1 -edge X-ray absorption, which exhibits $s \rightarrow p$ transitions, can provide additional information for determining the electronic state and geometry of the absorbing atom. Therefore, Re L_1 -edge XANES spectra were acquired under the aforementioned conditions. The Re L_1 -edge XANES spectra of the examined catalysts during the H_2 reduction were collected, along with those of reference compounds (**Figure 4**). Only NH_4ReO_4 was used as the reference compound for Re^{7+} because of its ease of handling. The pre-edge peak of the Re L_1 -edge XANES spectra was observed at approximately 12,527 eV in the spectra of NH_4ReO_4 and the supported Re samples treated at low temperatures (<200 °C), which was predominantly attributed to the forbidden $2s \rightarrow 5d$ electronic transition due to the mixing of Re and ligand p-orbitals into vacant d-orbitals caused by the less symmetric nature of Re (i.e., distortion from O_h symmetry). The edge positions and shapes of these spectra were identical, which indicated that the Re in these samples existed in a Re^{7+} form; this is consistent with the Re L_3 -edge XANES measurements. The absorption edge positions for $\text{Re}(5)/\text{TiO}_2$, $\text{Re}(5)/\text{SiO}_2$, $\text{Re}(5)/\text{ZrO}_2$, and $\text{Re}(5)/\text{V}_2\text{O}_5$ shifted to lower energies upon H_2 reduction at 300 °C, whereas those of the other Re species decreased at higher temperatures. These results indicate that the valency of the Re species decreased at 200–400 °C, except that of Re on MgO, where the shift was observed at temperatures above 500 °C.

LCF was performed on the set of XANES spectra to better illustrate the variations in the oxidation state following the H_2 reduction at a glance (**Figure 5**). Numerical data for the LCF results are available in

Supporting Information (**Table S1-S6**). The representative fitted data for Re(5)/TiO₂ treated at 100 °C, 500 °C, and 700 °C are also included in **Figure S12**. It is worth noting that the LCF results are not absolute and should only be considered as a qualitative approximation of the changes in the oxidation state. All the investigated catalysts underwent reduction at temperatures as low as 300 °C, as indicated by the increase in the fraction of Re⁰ species at 300 °C, except for Re(5)/MgO, whose reduction occurred at temperatures higher than 400 °C. These results are consistent with the reducibility trend of the Re species observed in the H₂-TPR profiles (**Figure 2**). Re(5)/ZrO₂ exhibited high reducibility of the Re species, showing a relatively lower fraction of Re⁷⁺ even at 100 °C. A sharp decrease in the Re⁷⁺ fraction, followed by an increase in the Re⁴⁺ and Re⁰ fractions, was observed at 300 °C. From 300 °C onwards, a gradual increase was observed in the Re⁰ fraction, which was accompanied by a gradual decrease in the Re⁴⁺ fraction, thereby confirming the occurrence of the reduction. A similar tendency was observed for Re(5)/TiO₂, Re(5)/SiO₂, and—to a lesser extent—for Re(5)/Al₂O₃ and Re(5)/V₂O₅, where a drastic decrease in the Re⁷⁺ fraction did not occur until 400 °C. Although Re(5)/MgO also showed a relatively low Re⁷⁺ fraction, the fraction of this high-valence species decreased slowly as the temperature increased, without the sharp decline observed for the other catalysts; this can be explained by the low reducibility of the Re species supported on MgO. Overall, the reducibility trends of the catalysts are in line with the H₂-TPR results presented in **Figure 2**. Although there can be several mechanisms to reduce the supported Re with H₂, the present study focusses on investigation of the states of the supported Re species made by the same experimental protocol. Note that some support materials can also be reduced during the H₂ reduction treatment as reported on a similar Re/TiO₂ system.⁷⁸

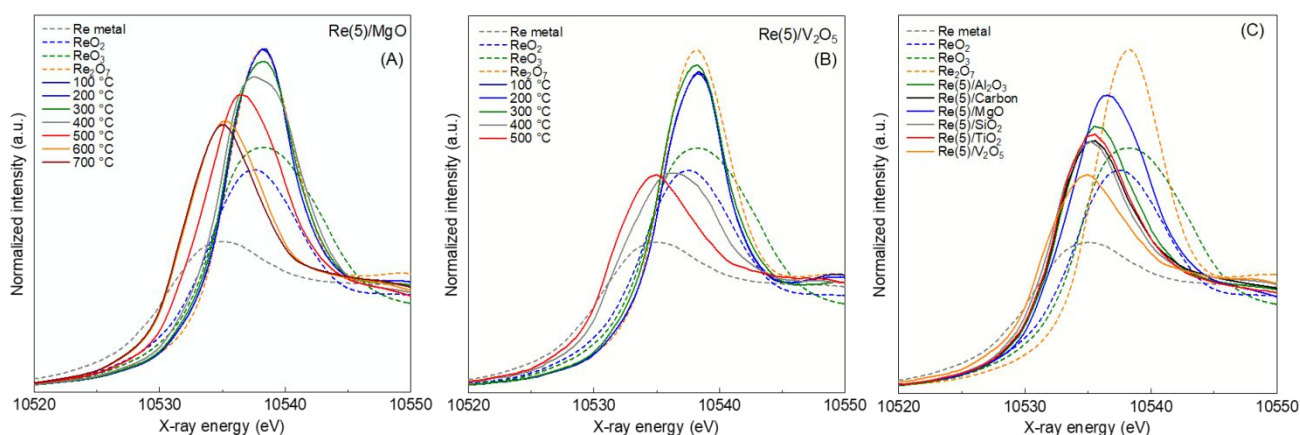


Figure 3. *In situ* Re L₃-edge XANES spectra of (A) Re(5)/MgO and (B) Re(5)/V₂O₅. Samples were heated under a flow of 5% H₂/He (100 mL min⁻¹) up to 700 °C at a heating rate of 10 °C min⁻¹. (C) Comparison of XANES spectra of Re on different supports that were acquired at 500 °C under a flow of 5% H₂/He (100 mL min⁻¹). XANES spectra of reference samples were recorded at room temperature. Spectra for Re(5)/TiO₂, Re(5)/Al₂O₃, Re(5)/SiO₂, and Re(5)/carbon are available in our previous work.⁷⁴

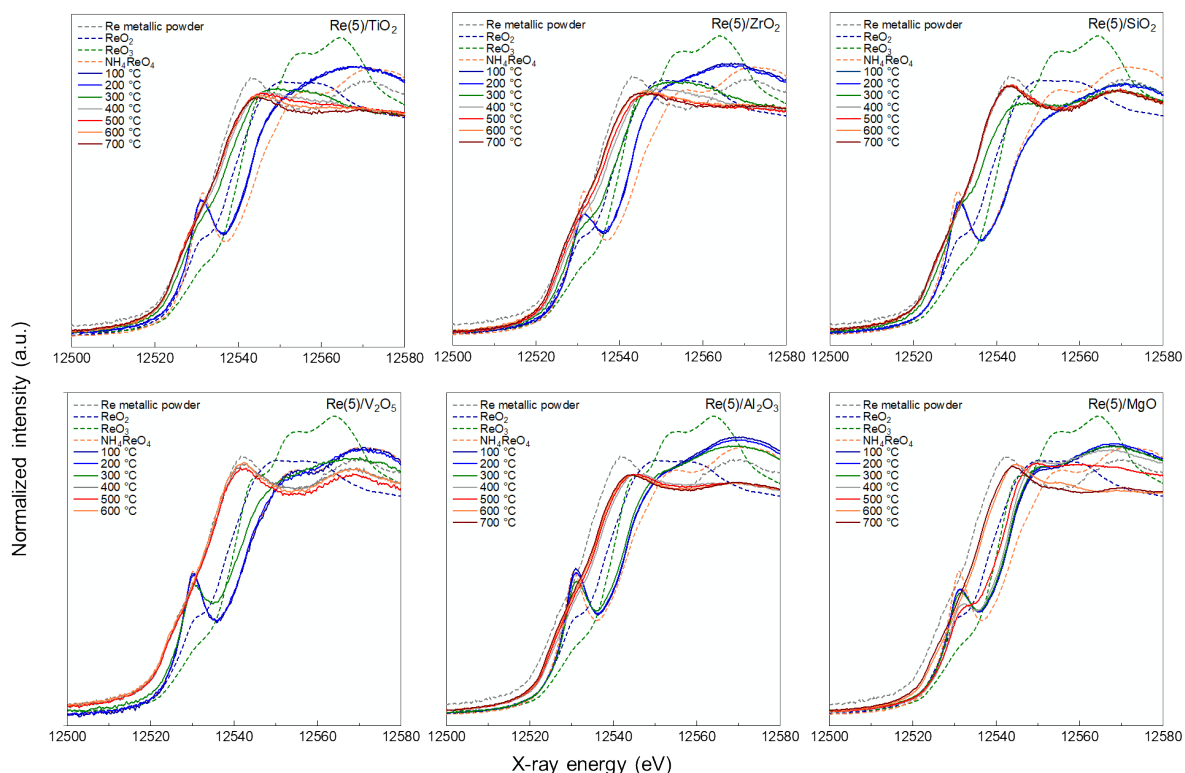


Figure 4. *In situ* Re L_1 -edge XANES spectra of Re(5)/support catalysts. Samples were heated under a flow of 5% H_2/He (100 mL min^{-1}) up to $700 \text{ }^\circ\text{C}$ at a heating rate of $10 \text{ }^\circ\text{C/min}$. XANES spectra of reference samples were recorded at room temperature.

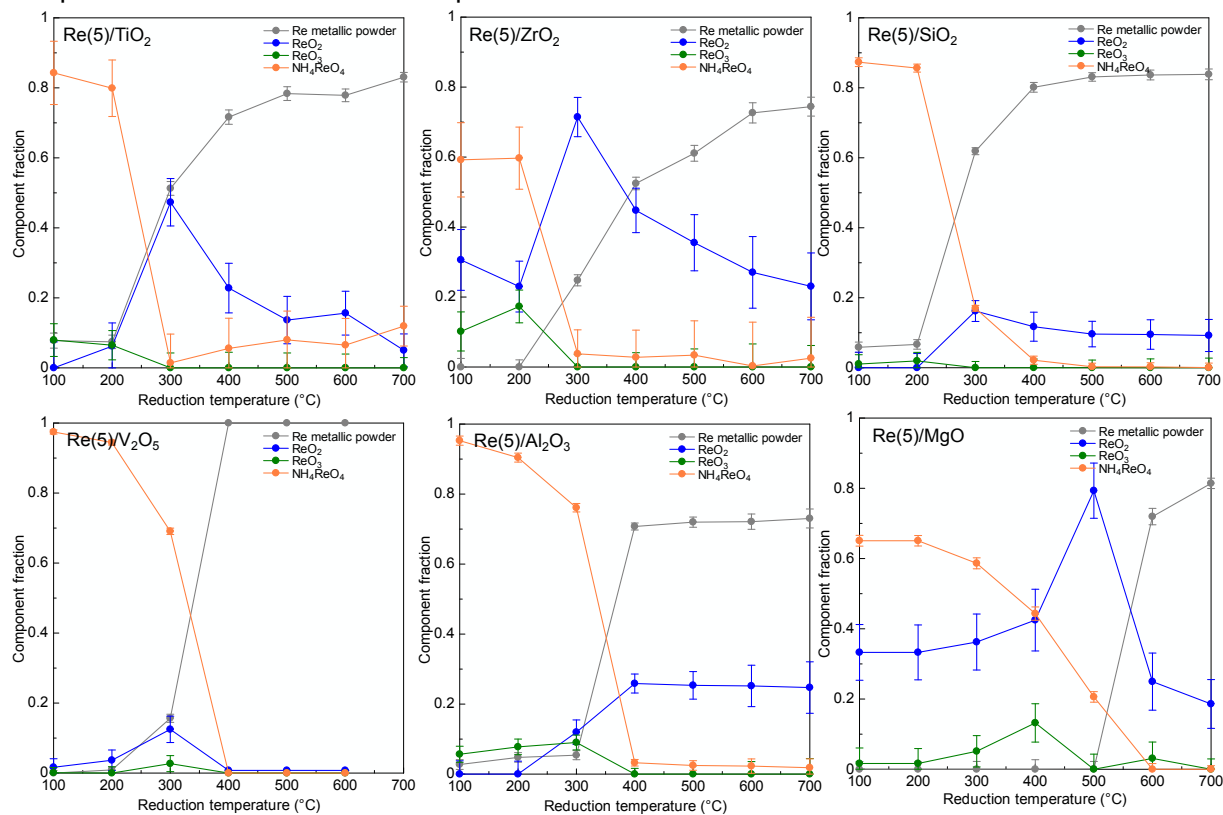


Figure 5. Linear combination fitting (LCF) results showing the component fraction of *in situ* Re L_1 -edge XANES spectra of Re(5)/support catalysts. LCF was performed on spectra available in **Figure 4** over a fitting range of -20 to 30 eV relative to the absorption edge (E_0) using Re powder (Re^0), ReO_2 (Re^{4+}), ReO_3 (Re^{6+}), and NH_4ReO_4 (Re^{7+}) as standards.

The FTIR spectra of CO adsorbed on the different Re(5)/support catalysts are shown in **Figure 6**. The assignments for the CO adsorption bands are listed in **Table 1**. Among all the investigated catalysts, the CO adsorption spectrum of Re(5)/TiO₂ showed the highest number of peaks with seven distinctive adsorption bands. The CO adsorption band with the highest intensity at 2038 cm⁻¹ was present in the spectra of both Re(5)/ZrO₂ and Re(5)/TiO₂, which was assigned to linearly bonded CO on Re or Re(CO)₃.^{79–82} Moreover, the bands at 1945 and 1880 cm⁻¹ were ascribed to bridged CO adsorbed on Re or Re(CO)₃.^{79–82} Re(CO)₃ is presumably a more appropriate assignment, given the prevalence of highly dispersed Re species in both the samples. Interestingly, the bands in the Re(5)/Al₂O₃ and Re(5)/MgO spectra shifted slightly to lower frequencies; these bands were assumed to represent linear and bridged CO on Re, respectively, because large Re nanoparticles (up to 4 nm in size) were present on both the catalysts (**Figure S4**). However, the possibility of these bands being derived from Re(CO)₃ species cannot be discounted, and the slight difference in peak position might stem from the influence of different support materials, as reported by Komiyama et al.⁸⁰ Peaks representing CO adsorbed on Re species were absent from the Re(5)/V₂O₅ and Re(5)/SiO₂ spectra. In the Re(5)/TiO₂ spectrum, the band at 2158 cm⁻¹ was assigned to CO bonded on reduced TiO₂, as reported by Liao et al.,⁸³ whereas those at 2116, 2056, and 2003 cm⁻¹ were ascribed to Re₂(CO)₁₀ based on studies on the Re/Al₂O₃ catalyst conducted by Solymosi et al.⁷⁹ and Anderson et al.⁸⁴

CO adsorption was also performed on Re(5)/TiO₂ pre-treated at different temperatures (See **Figures S8-S11** for HAADF-STEM images), and the corresponding FTIR spectra were acquired (**Figure 7**). The unreduced sample showed no CO adsorption bands, suggesting that CO adsorption only occurred on the reduced surface species. Minor CO adsorption bands with weak intensities appeared at 2116 and ~2035 cm⁻¹ in the spectrum of the sample reduced at 300 °C. The samples pretreated at 700 °C showed multiple prominent absorption bands similar to those of the samples pretreated at 500 °C, albeit with considerably weaker intensities. However, as the pretreatment temperature increased to 900 °C, most of the adsorption bands disappeared, except for a weak band at 2116 cm⁻¹. This phenomenon can be attributed to the strong MSIs⁸ at elevated temperatures that limit the access to surface species, thereby preventing CO adsorption. Additional CO adsorption experiment was performed for Re(5)/ZrO₂ and Re(5)/Al₂O₃ pre-treated at different temperatures, as shown in **Figure S13**. Similar trend of reduction temperatures on the CO adsorption as for the Re(5)/TiO₂ system were observed.

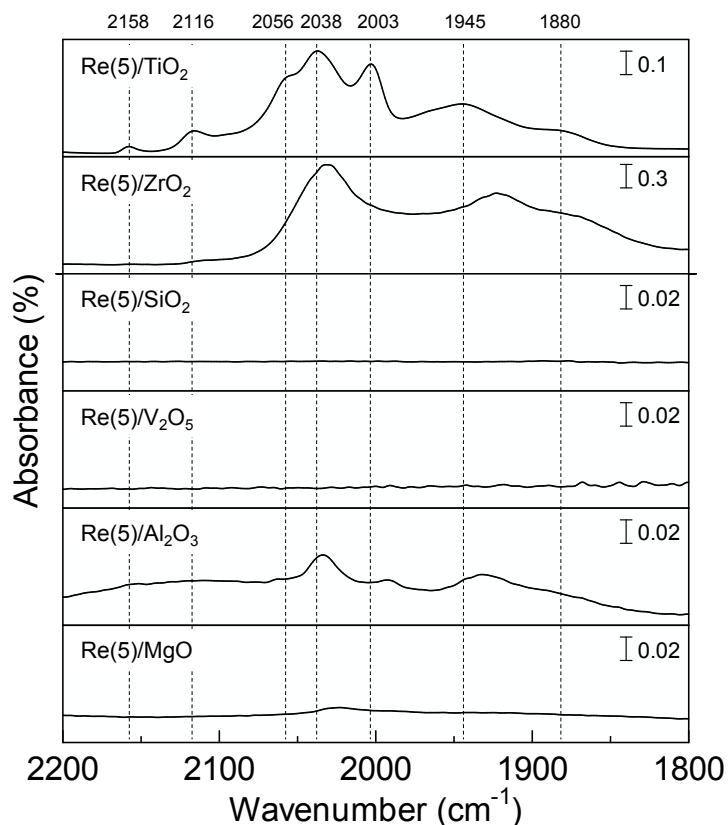


Figure 6. FTIR spectra of CO adsorbed on Re(5)/support catalysts after H₂ reduction. Each sample was pretreated at 500 °C under a flow 10% H₂/He (100 mL min⁻¹) for 30 min, exposed to a flow of 1% CO/He (100 mL min⁻¹) for 5 min, and purged with He for 5 min.

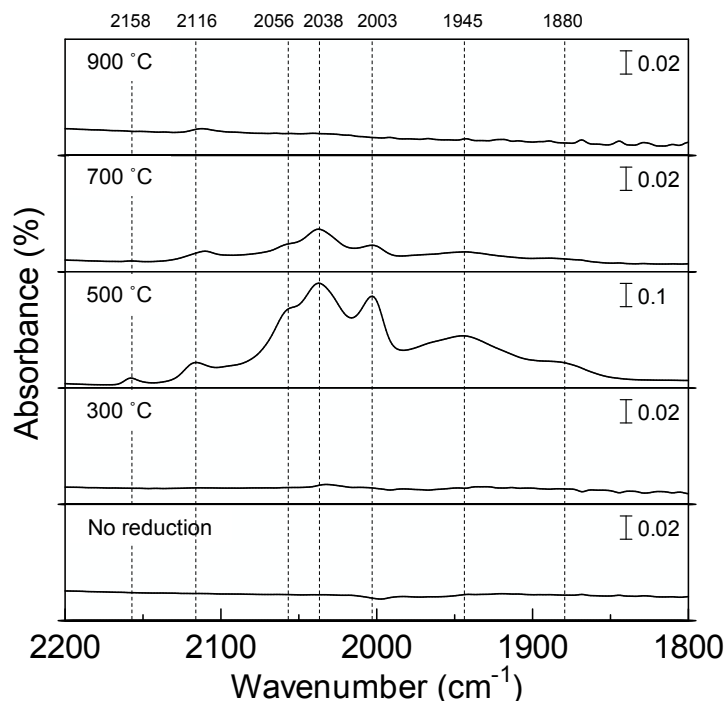


Figure 7. FTIR spectra of CO adsorbed on un-reduced and H₂-reduced Re(5)/TiO₂ catalysts. Each sample was pretreated (if applicable) under a flow of 10% H₂/He (100 mL min⁻¹) for 30 min, exposed to a flow of 1% CO/He (100 mL min⁻¹) for 5 min, and purged with He for 5 min.

Table 1. Assignment of peaks appearing in the IR spectra of CO adsorbed on the Re(5)/support catalysts.

Wavenumber (cm ⁻¹)	Assignment	Reference
2158	CO on Ti ³⁺	83
2116	Re ₂ (CO) ₁₀	79,84
2056	Re ₂ (CO) ₁₀	79,84
2038	Linear CO, Re(CO) ₃ , Re ₂ (CO) ₁₀	79–82
2003	Re(CO) ₃ , Re ₂ (CO) ₁₀	79,84
1945	Bridged CO, Re(CO) ₃ , Re ₂ (CO) ₁₀	79–82
1880	Bridged CO, Re(CO) ₃	79–82

DFT calculations and XANES simulations

To clarify the effects of the Re cluster structure on the XANES spectra, XANES simulations were performed using the model structures obtained by DFT calculations with the FDMNES software.⁸⁵ **Figure 8(a)** shows the simulated Re L_3 -edge XANES spectra of the supported Re clusters and the Re slab model that represents large nanoparticles. The white-line intensity of the catalysts decreased with increasing cluster size, although their formal oxidation states were all zero. This result indicates that the Re L_3 -edge XANES spectra were related not only to the valence states but also to the size of Re, which is consistent with our experimental data⁷⁶ and the simulation results of a Re/Al₂O₃ system reported by Bare et al.⁷⁷

Figure 8(b) shows the simulated Re L_1 -edge XANES spectra of the different catalyst configurations. The absorption-edge positions of all the supported Re clusters, except for Re₁/TiO₂, were similar to those of the metallic Re(0001) model. The simulated Re L_1 -edge spectrum of Re₁/TiO₂ showed a pre-edge shoulder peak, and its absorption shifted to a higher energy. Bader charge analysis was also performed to determine the valence state of Re in the simulated structures, with bulk ReO₂ used as the reference compound. The average Bader charges of Re(0001), Re₂₀/TiO₂, Re₁₃/TiO₂, Re₃/TiO₂, Re₁/TiO₂, and ReO₂ were calculated to be 0.00, 0.13, 0.14, 0.40, 0.79, and 1.85, respectively (**Table S7**). Although the formal oxidation states for the Re species were considered, except that of ReO₂, the Bader charge values were positive up to 0.79, indicating that the Re clusters were electron deficient owing to their highly dispersed nature, especially those with fewer Re atoms. This is reflected more strongly in the Re L_3 -edge XANES spectra than in the Re L_1 -edge XANES spectra because the white-line intensity depends directly on the 5d occupation number. Although there are limitations to the computational accuracy and the variety of metal-oxide surfaces, the level of theory should be sufficient to qualitatively capture the trends discussed in this study. The presented systematic investigation can nevertheless be expected to be a helpful guide for designing heterogeneous metal-oxide catalysts.

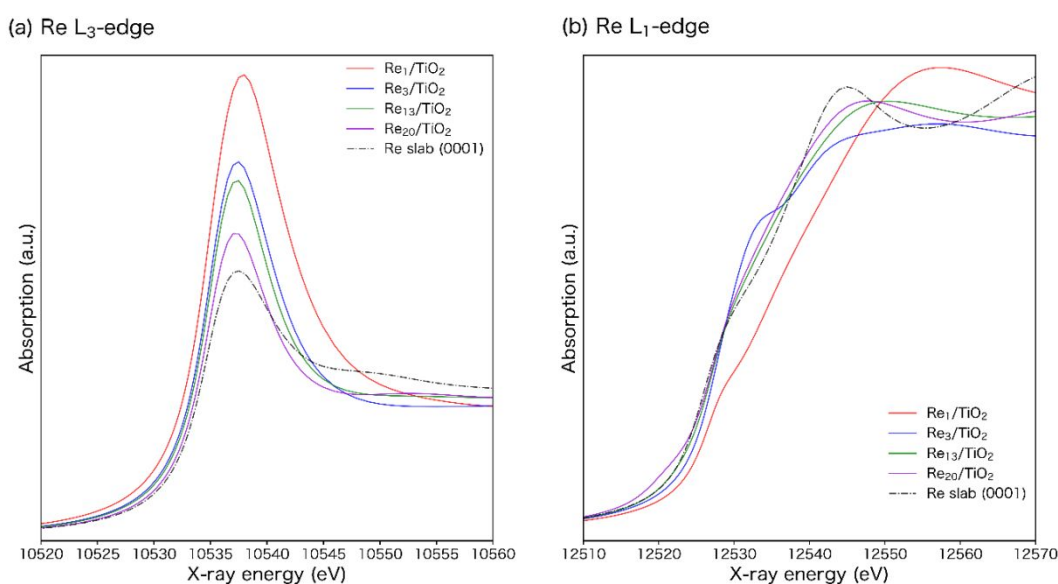


Figure 8. Simulated (a) Re L_3 -edge and (b) Re L_1 -edge XANES spectra of the DFT-optimized Re(0001) slab, Re₁/TiO₂, Re₃/TiO₂, Re₁₃/TiO₂, and Re₂₀/TiO₂ structures constructed using FDMNES software.

Conclusion

The reducibility and oxidation states of 5 wt.% Re supported on various oxide supports, including TiO₂, SiO₂, Al₂O₃, MgO, V₂O₅, and ZrO₂, were investigated in this study using experimental and computational approaches. The Re species started to exhibit lower valency at 200–400 °C upon H₂ reduction, except the Re on MgO, where the shift was observed at temperatures above 400 °C. Additionally, the dependence of the Re L₃- and L₁-edge XANES spectra on the Re size was investigated, which revealed that the L₃-edge was more sensitive than the L₁-edge to the size of the Re clusters because of the direct dependence of the white-line intensity on the 5d occupation number.

Conflicts of interest

There are no conflicts to declare.

Acknowledgements

This study was financially supported by JSPS KAKENHI grants (20H02518, 20H02775, 20KK0111, 20F20345, 21K18185, 22J11825, and 22K14538) and a JST-CREST project (JPMJCR17J3). The authors are grateful to the technical staff at the Open Facility of Hokkaido University for their assistance with the STEM observations. All DFT calculations were performed using supercomputers at RIIT (Kyushu University) and ACCMS (Kyoto University).

References

- 1 I. Ro, J. Resasco and P. Christopher, Approaches for Understanding and Controlling Interfacial Effects in Oxide-Supported Metal Catalysts, *ACS Catal.*, 2018, **8**, 7368–7387.
- 2 L. Zhang, M. Zhou, A. Wang and T. Zhang, Selective Hydrogenation over Supported Metal Catalysts: From Nanoparticles to Single Atoms, *Chem. Rev.*, 2020, **120**, 683–733.
- 3 M. Haruta, Size- and support-dependency in the catalysis of gold, *Catal. Today*, 1997, **36**, 153–166.
- 4 H. J. Freund and G. Pacchioni, Oxide ultra-thin films on metals: New materials for the design of supported metal catalysts, *Chem. Soc. Rev.*, 2008, **37**, 2224–2242.
- 5 E. D. Goodman, J. A. Schwalbe and M. Cargnello, Mechanistic understanding and the rational design of sinter-resistant heterogeneous catalysts, *ACS Catal.*, 2017, **7**, 7156–7173.
- 6 M. Haruta, Spiers Memorial Lecture: Role of perimeter interfaces in catalysis by gold nanoparticles, *Faraday Discuss.*, 2011, **152**, 11–32.
- 7 M. Cargnello, V. V. T. Doan-Nguyen, T. R. Gordon, R. E. Diaz, E. A. Stach, R. J. Gorte, P. Fornasiero and C. B. Murray, Control of metal nanocrystal size reveals metal-support interface role for ceria catalysts, *Science (80-.)*, 2013, **341**, 771–773.
- 8 T. W. van Deelen, C. Hernández Mejía and K. P. de Jong, Control of metal-support interactions in heterogeneous catalysts to enhance activity and selectivity, *Nat. Catal.*, 2019, **2**, 955–970.
- 9 D. W. Goodman, Model Studies in Catalysis Using Surface Science Probes, *Chem. Rev.*, 1995, **95**, 523–536.
- 10 S. Mostafa, F. Behafarid, J. R. Croy, L. K. Ono, L. Li, J. C. Yang, A. I. Frenkel and B. R. Cuenya, Shape-dependent catalytic properties of Pt nanoparticles, *J. Am. Chem. Soc.*, 2010, **132**, 15714–15719.
- 11 L. Liu and A. Corma, Metal Catalysts for Heterogeneous Catalysis: From Single Atoms to Nanoclusters and Nanoparticles, *Chem. Rev.*, 2018, **118**, 4981–5079.
- 12 T. W. Hansen, A. T. Delariva, S. R. Challa and A. K. Datye, Sintering of catalytic nanoparticles: Particle migration or Ostwald ripening?, *Acc. Chem. Res.*, 2013, **46**, 1720–1730.
- 13 Y. Q. Su, J. X. Liu, I. A. W. Filot and E. J. M. Hensen, Theoretical Study of Ripening Mechanisms of Pd Clusters on Ceria, *Chem. Mater.*, 2017, **29**, 9456–9462.
- 14 S. K. Iyemperumal, T. D. Pham, J. Bauer and N. A. Deskins, Quantifying Support Interactions and Reactivity Trends of Single Metal Atom Catalysts over TiO₂, *J. Phys. Chem. C*, 2018, **122**, 25274–25289.
- 15 R. Rousseau, V. A. Glezakou and A. Selloni, Theoretical insights into the surface physics and chemistry of redox-active oxides, *Nat. Rev. Mater.*, 2020, **5**, 460–475.
- 16 N. D. Spencer and G. A. Somorjai, Ammonia Synthesis Catalyzed by Rhenium, *J. Catal.*, 1982, **72**, 142–146.
- 17 N. Ota, M. Tamura, Y. Nakagawa, K. Okumura and K. Tomishige, Hydrodeoxygenation of vicinal OH groups over heterogeneous rhenium catalyst promoted by palladium and ceria support, *Angew. Chemie - Int. Ed.*, 2015, **54**, 1897–1900.

- 18 L. Ma, K. Sun, M. Luo, L. Yan, Z. Jiang, A. H. Lu and Y. Ding, Role of ReO Species in Ni-Re/Al₂O₃ Catalyst for Amination of Monoethanolamine, *J. Phys. Chem. C*, 2018, **122**, 23011–23025.
- 19 X. Huang, K. Liu, W. L. Vrijburg, X. Ouyang, A. Iulian Dugulan, Y. Liu, M. W. G. M. Tiny Verhoeven, N. A. Kosinov, E. A. Pidko and E. J. M. Hensen, Hydrogenation of levulinic acid to γ -valerolactone over Fe-Re/TiO₂ catalysts, *Appl. Catal. B Environ.*, 2020, **278**, 119314.
- 20 J. Cao, M. Tamura, R. Hosaka, A. Nakayama, J. Y. Hasegawa, Y. Nakagawa and K. Tomishige, Mechanistic Study on Deoxydehydration and Hydrogenation of Methyl Glycosides to Dideoxy Sugars over a ReO_x-Pd/CeO₂ Catalyst, *ACS Catal.*, 2020, **10**, 12040–12051.
- 21 B. Zhang and I. E. Wachs, Identifying the catalytic active site for propylene metathesis by supported ReO_x catalysts, *ACS Catal.*, 2021, **11**, 1962–1976.
- 22 J. Qi, J. Finzel, H. Robotjazi, M. Xu, A. S. Hoffman, S. R. Bare, X. Pan and P. Christopher, Selective Methanol Carbonylation to Acetic Acid on Heterogeneous Atomically Dispersed ReO₄/SiO₂ Catalysts, *J. Am. Chem. Soc.*, 2020, **142**, 14178–14189.
- 23 J. D. Kammert, A. Chemburkar, N. Miyake, M. Neurock and R. J. Davis, Reaction Kinetics and Mechanism for the Catalytic Reduction of Propionic Acid over Supported ReO_x Promoted by Pd, *ACS Catal.*, 2021, **11**, 1435–1455.
- 24 B. Hočevár, A. Prašnikar, M. Huš, M. Grilc and B. Likozar, H₂ - Free Re - Based Catalytic Dehydroxylation of Aldaric Acid to Muconic and Adipic Acid Esters, *Angew. Chemie*, 2021, **133**, 1264–1273.
- 25 M. L. Gothe, K. L. C. Silva, A. L. Figueredo, J. L. Fiorio, J. Rozendo, B. Manduca, V. Simizu, R. S. Freire, M. A. S. Garcia and P. Vidinha, Rhenium – A Tuneable Player in Tailored Hydrogenation Catalysis, *Eur. J. Inorg. Chem.*, 2021, **39**, 4043–4065.
- 26 L. Wang, R. Ohnishi and M. Ichikawa, Selective Dehydroaromatization of Methane toward Benzene on Re/HZSM-5 Catalysts and Effects of CO/CO₂ Addition, *J. Catal.*, 2000, **190**, 276–283.
- 27 M. Chia, Y. J. Pagán-Torres, D. Hibbitts, Q. Tan, H. N. Pham, A. K. Datye, M. Neurock, R. J. Davis and J. A. Dumesic, Selective hydrogenolysis of polyols and cyclic ethers over bifunctional surface sites on rhodium-rhenium catalysts, *J. Am. Chem. Soc.*, 2011, **133**, 12675–12689.
- 28 X. She, H. M. Brown, X. Zhang, B. K. Ahring and Y. Wang, Selective hydrogenation of trans,trans-muconic acid to adipic acid over a titania-supported rhenium catalyst, *ChemSusChem*, 2011, **4**, 1071–1073.
- 29 S. Lwin, Y. Li, A. I. Frenkel and I. E. Wachs, Activation of Surface ReO_x Sites on Al₂O₃ Catalysts for Olefin Metathesis, *ACS Catal.*, 2015, **5**, 6807–6814.
- 30 L. Sandbrink, E. Klindtworth, H. U. Islam, A. M. Beale and R. Palkovits, ReO_x/TiO₂: A Recyclable Solid Catalyst for Deoxydehydration, *ACS Catal.*, 2016, **6**, 677–680.
- 31 K. Yamaguchi, J. Cao, M. Betchaku, Y. Nakagawa, M. Tamura, A. Nakayama, M. Yabushita and K. Tomishige, Deoxydehydration of Biomass-Derived Polyols Over Silver-Modified Ceria-Supported Rhenium Catalyst with Molecular Hydrogen, *ChemSusChem*, 2022, **15**, e202102663.
- 32 Y. Takeda, Y. Nakagawa and K. Tomishige, Selective hydrogenation of higher saturated carboxylic

- acids to alcohols using a $\text{ReO}_x\text{-Pd/SiO}_2$ catalyst, *Catal. Sci. Technol.*, 2012, **2**, 2221–2223.
- 33 K. Liu, J. Pritchard, L. Lu, R. Van Putten, M. W. G. M. Verhoeven, M. Schmitkamp, X. Huang, L. Lefort, C. J. Kiely, E. J. M. Hensen and E. A. Pidko, Supported nickel-rhenium catalysts for selective hydrogenation of methyl esters to alcohols, *Chem. Commun.*, 2017, **53**, 9761–9764.
- 34 T. Toyao, S. M. A. H. Siddiki, A. S. Touchy, W. Onodera, K. Kon, Y. Morita, T. Kamachi, K. Yoshizawa and K. Shimizu, TiO_2 -Supported Re as a General and Chemoselective Heterogeneous Catalyst for Hydrogenation of Carboxylic Acids to Alcohols, *Chem. - A Eur. J.*, 2017, **23**, 1001–1006.
- 35 T. Toyao, S. M. A. H. Siddiki, Y. Morita, T. Kamachi, A. S. Touchy, W. Onodera, K. Kon, S. Furukawa, H. Ariga, K. Asakura, K. Yoshizawa and K. Shimizu, Rhenium-Loaded TiO_2 : A Highly Versatile and Chemoselective Catalyst for the Hydrogenation of Carboxylic Acid Derivatives and the N-Methylation of Amines Using H_2 and CO_2 , *Chem. - A Eur. J.*, 2017, **23**, 14848–14859.
- 36 K. Tomishige, Y. Nakagawa and M. Tamura, Taming heterogeneous rhenium catalysis for the production of biomass-derived chemicals, *Chinese Chem. Lett.*, 2020, **31**, 1049–1344.
- 37 T. Iizuka, M. Kojima and K. Tanabe, Support effects in the formation of methanol from carbon dioxide and hydrogen over rhenium catalysts, *J. Chem. Soc. Chem. Commun.*, 1983, 638–639.
- 38 Z. Xu, Z. H. Qian, K. Tanabe and H. Hattori, Support Effect of Re Catalyst on Methanol Synthesis From CO_2 and H_2 Under a Pressure of 5 atm, *Bull. Chem. Soc. Jpn.*, 1991, **64**, 1664–1668.
- 39 H. G. Manyar, C. Paun, R. Pilus, D. W. Rooney, J. M. Thompson and C. Hardacre, Highly selective and efficient hydrogenation of carboxylic acids to alcohols using titania supported Pt catalysts, *Chem. Commun.*, 2010, **46**, 6279–6281.
- 40 B. Rozmysłowicz, A. Kirilin, A. Aho, H. Manyar, C. Hardacre, J. Wärnå, T. Salmi and D. Y. Murzin, Selective Hydrogenation of Fatty Acids to Alcohols over Highly Dispersed $\text{ReO}_x/\text{TiO}_2$ Catalyst, *J. Catal.*, 2015, **328**, 197–207.
- 41 K. W. Ting, T. Toyao, S. M. A. H. Siddiki and K. Shimizu, Low-Temperature Hydrogenation of CO_2 to Methanol over Heterogeneous TiO_2 -Supported Re Catalysts, *ACS Catal.*, 2019, **9**, 3685–3693.
- 42 K. W. Ting, H. Kamakura, S. Poly, T. Toyao, S. M. A. H. Siddiki, Z. Maeno, K. Matsushita and K. Shimizu, Catalytic Methylation of Aromatic Hydrocarbons using CO_2/H_2 over Re/TiO_2 and H - MOR catalysts, *ChemCatChem*, 2020, **12**, 2215–2220.
- 43 M. L. Gothe, F. J. Pérez-Sanz, A. H. Braga, L. R. Borges, T. F. Abreu, R. C. Bazito, R. V. Gonçalves, L. M. Rossi and P. Vidinha, Selective CO_2 hydrogenation into methanol in a supercritical flow process, *J. CO2 Util.*, 2020, **40**, 101195.
- 44 M. F. L. Johnson and V. M. LeRoy, The state of rhenium in Pt/Re/alumina catalysts, *J. Catal.*, 1974, **35**, 434–440.
- 45 S. Tatarenko, P. Dolle, R. Morancho, M. Alnot, J. J. Ehrhardt and R. Ducros, XPS and UPS study of oxygen adsorption on $\text{Re}(0001)$ at low temperatures, *Surf. Sci.*, 1983, **134**, L505–L512.
- 46 H. Peled and M. Asscher, Dissociative chemisorption of CO_2 on a $\text{Re}(0001)$ single crystal surface, *Surf. Sci.*, 1987, **183**, 201–215.
- 47 A. S. Y. Chan, W. Chen, H. Wang, J. E. Rowe and T. E. Madey, Methanol reactions over oxygen-

- modified re surfaces: Influence of surface structure and oxidation, *J. Phys. Chem. B*, 2004, **108**, 14643–14651.
- 48 S. Koso, H. Watanabe, K. Okumura, Y. Nakagawa and K. Tomishige, Stable low-valence ReO_x cluster attached on Rh metal particles formed by hydrogen reduction and its formation mechanism, *J. Phys. Chem. C*, 2012, **116**, 3079–3090.
- 49 K. Hahn and M. Mavrikakis, Atomic and molecular adsorption on Re(0001), *Top. Catal.*, 2014, **57**, 54–68.
- 50 J. Lin, L. Yang, T. Wang and R. Zhou, Investigation on the structure-activity relationship of BaO promoting Pd/CeO₂-ZrO₂ catalysts for CO, HC and NO_x conversions, *Phys. Chem. Chem. Phys.*, 2017, **19**, 7844–7852.
- 51 S. R. Bare, F. D. Vila, M. E. Charochak, S. Prabhakar, W. J. Bradley, C. Jaye, D. A. Fischer, S. T. Hayashi, S. A. Bradley and J. J. Rehr, Characterization of Coke on a Pt-Re/ γ -Al₂O₃ Re-Forming Catalyst: Experimental and Theoretical Study, *ACS Catal.*, 2017, **7**, 1452–1461.
- 52 M. T. Greiner, T. C. R. Rocha, B. Johnson, A. Klyushin, A. Knop-Gericke and R. Schlögl, The oxidation of rhenium and identification of rhenium oxides during catalytic partial oxidation of ethylene: An in-situ XPS study, *Zeitschrift für Phys. Chemie*, 2014, **228**, 521–541.
- 53 R. J. Lobo-Lapidus and B. C. Gates, Rhenium complexes and clusters supported on γ -Al₂O₃: Effects of rhenium oxidation state and rhenium cluster size on catalytic activity for n-butane hydrogenolysis, *J. Catal.*, 2009, **268**, 89–99.
- 54 B. Mitra, X. Gao, I. E. Wachs, a. M. Hirt and G. Deo, Characterization of supported rhenium oxide catalysts: effect of loading, support and additives, *Phys. Chem. Chem. Phys.*, 2001, **3**, 1144–1152.
- 55 J. Okal, L. K. Episki, L. Krajczyk and W. Tylus, Oxidation and redispersion of a low-loaded Re/ γ -Al₂O₃ catalyst, *J. Catal.*, 2003, **219**, 362–371.
- 56 J. Okal, A study of effect of particle size on the oxidation of rhenium in the Re/ γ -Al₂O₃ catalysts, *Appl. Catal. A Gen.*, 2005, **287**, 214–220.
- 57 X. She, J. H. Kwak, J. Sun, J. Hu, M. Y. Hu, C. Wang, C. H. F. Peden and Y. Wang, Highly dispersed and active reo x on alumina-modified SBA-15 silica for 2-butanol dehydration, *ACS Catal.*, 2012, **2**, 1020–1026.
- 58 D. D. Falcone, J. H. Hack, A. Y. Klyushin, A. Knop-Gericke, R. Schlögl and R. J. Davis, Evidence for the Bifunctional Nature of Pt-Re Catalysts for Selective Glycerol Hydrogenolysis, *ACS Catal.*, 2015, **5**, 5679–5695.
- 59 B. K. Ly, B. Tapin, M. Aouine, P. Delichere, F. Epron, C. Pinel, C. Especel and M. Besson, Insights into the Oxidation State and Location of Rhenium in Re-Pd/TiO₂ Catalysts for Aqueous-Phase Selective Hydrogenation of Succinic Acid to 1,4-Butanediol as a Function of Palladium and Rhenium Deposition Methods, *ChemCatChem*, 2015, **7**, 2161–2178.
- 60 S. T. Thompson and H. H. Lamb, Catalysts for selective hydrogenation of furfural derived from the double complex salt [Pd(NH₃)₄](ReO₄)₂ on γ -Al₂O₃, *J. Catal.*, 2017, **350**, 111–121.
- 61 X. Di, C. Li, G. Lafaye, C. Especel, F. Epron and C. Liang, Influence of Re-M interactions in Re-M/C

- bimetallic catalysts prepared by a microwave-assisted thermolytic method on aqueous-phase hydrogenation of succinic acid, *Catal. Sci. Technol.*, 2017, **7**, 5212–5223.
- 62 Y. Nakagawa, S. Tazawa, T. Wang, M. Tamura, N. Hiyoshi, K. Okumura and K. Tomishige, Mechanistic Study of Hydrogen-Driven Deoxydehydration over Ceria-Supported Rhenium Catalyst Promoted by Au Nanoparticles, *ACS Catal.*, 2018, **8**, 584–595.
- 63 B. E. Sharkey and F. C. Jentoft, Fundamental Insights into Deactivation by Leaching during Rhenium-Catalyzed Deoxydehydration, *ACS Catal.*, 2019, **9**, 11317–11328.
- 64 S. Mine, K. W. Ting, L. Li, Y. Hinuma, Z. Maeno, S. M. A. H. Siddiki, T. Toyao and K. Shimizu, Experimental and Theoretical Investigation of Metal-Support Interactions in Metal-Oxide-Supported Rhenium Materials, *J. Phys. Chem. C*, 2022, **126**, 4472–4482.
- 65 O. Bunău and Y. Joly, Self-consistent aspects of x-ray absorption calculations, *J. Phys. Condens. Matter*, 2009, **21**, 345501.
- 66 J. D. Bourke, C. T. Chantler and Y. Joly, FDMX: Extended X-ray absorption fine structure calculations using the finite difference method, *J. Synchrotron Radiat.*, 2016, **23**, 551–559.
- 67 C. Liu, H. Kubota, T. Amada, K. Kon, T. Toyao, Z. Maeno, K. Ueda, J. Ohyama, A. Satsuma, T. Tanigawa, N. Tsunoji, T. Sano and K. ichi Shimizu, In Situ Spectroscopic Studies on the Redox Cycle of NH₃-SCR over Cu-CHA Zeolites, *ChemCatChem*, 2020, **12**, 3050–3059.
- 68 B. Ravel and M. Newville, ATHENA, ARTEMIS, HEPHAESTUS: Data analysis for X-ray absorption spectroscopy using IFEFFIT, *J. Synchrotron Radiat.*, 2005, **12**, 537–541.
- 69 G. Kresse and J. Furthmüller, Efficient iterative schemes for ab initio total-energy calculations using a plane-wave basis set, *Phys. Rev. B - Condens. Matter Mater. Phys.*, 1996, **54**, 11169–11186.
- 70 G. Kresse and J. Furthmüller, Efficiency of ab-initio total energy calculations for metals and semiconductors using a plane-wave basis set, *Comput. Mater. Sci.*, 1996, **6**, 15–50.
- 71 J. P. Perdew, A. Ruzsinszky, G. I. Csonka, O. A. Vydrov, G. E. Scuseria, L. A. Constantin, X. Zhou and K. Burke, Restoring the density-gradient expansion for exchange in solids and surfaces, *Phys. Rev. Lett.*, 2008, **100**, 136406.
- 72 P. E. Blöchl, Projector augmented-wave method, *Phys. Rev. B*, 1994, **50**, 17953–17979.
- 73 S. Grimme, S. Ehrlich and L. Goerigk, Effect of the damping function in dispersion corrected density functional theory, *J. Comput. Chem.*, 2011, **32**, 1456–1465.
- 74 Y. Hinuma, T. Toyao, T. Kamachi, Z. Maeno, S. Takakusagi, S. Furukawa, I. Takigawa and K. Shimizu, Density Functional Theory Calculations of Oxygen Vacancy Formation and Subsequent Molecular Adsorption on Oxide Surfaces, *J. Phys. Chem. C*, 2018, **122**, 29435–29444.
- 75 A. Jain, S. P. Ong, G. Hautier, W. Chen, W. D. Richards, S. Dacek, S. Cholia, D. Gunter, D. Skinner, G. Ceder and K. A. Persson, Commentary: The materials project: A materials genome approach to accelerating materials innovation, *APL Mater.*, 2013, **1**, 011002.
- 76 T. Toyao, K. W. Ting, S. M. A. H. Siddiki, A. S. Touchy, W. Onodera, Z. Maeno, H. Ariga-Miwa, Y. Kanda, K. Asakura and K. Shimizu, Mechanistic study of the selective hydrogenation of carboxylic acid derivatives over supported rhenium catalysts, *Catal. Sci. Technol.*, 2019, **9**, 5413–5424.

- 77 S. R. Bare, S. D. Kelly, F. D. Vila, E. Boldingh, E. Karapetrova, J. Kas, G. E. Mickelson, F. S. Modica, N. Yang and J. J. Rehr, Experimental (XAS, STEM, TPR, and XPS) and theoretical (DFT) characterization of supported rhenium catalysts, *J. Phys. Chem. C*, 2011, **115**, 5740–5755.
- 78 K. W. Ting, Z. Maeno, S. M. A. Hakim Siddiki, K. I. Shimizu and T. Toyao, Reverse water-gas shift reaction via redox of re nanoclusters supported on TiO₂, *Chem. Lett.*, 2021, **50**, 158–161.
- 79 F. Solymosi and T. Bánsági, CO-induced changes in structure of supported rhenium, *J. Phys. Chem.*, 1992, **96**, 1349–1355.
- 80 M. Komiyama, K. Vamamoto and Y. Ogino, Preparation of supported rhenium carbonyls and their characterization by IR and XPS studies, *J. Mol. Catal.*, 1989, **56**, 78–85.
- 81 H. Iida and A. Igarashi, Difference in the reaction behavior between Pt-Re/TiO₂ (Rutile) and Pt-Re/ZrO₂ catalysts for low-temperature water gas shift reactions, *Appl. Catal. A Gen.*, 2006, **303**, 48–55.
- 82 G. Braca, A. M. R. Galletti, G. Sbrana, M. Lami and M. Marchionna, Hydrogenolysis of formic esters with homogeneous and heterogeneous rhenium catalysts, *J. Mol. Catal. A Chem.*, 1995, **95**, 19–26.
- 83 L. F. Liao, C. F. Lien, D. L. Shieh, M. T. Chen and J. L. Lin, FTIR study of adsorption and photoassisted oxygen isotopic exchange of carbon monoxide, carbon dioxide, carbonate, and formate on TiO₂, *J. Phys. Chem. B*, 2002, **106**, 11240–11245.
- 84 J. A. Anderson, F. K. Chong and C. H. Rochester, IR study of CO adsorption on Pt, Re and Pt-Re/Al₂O₃ catalysts before and after coking, *J. Mol. Catal. A Chem.*, 1999, **140**, 65–80.
- 85 A. Tougeri, S. Cristol, E. Berrier, V. Briois, C. La Fontaine, F. Villain and Y. Joly, XANES study of rhenium oxide compounds at the L1 and L 3 absorption edges, *Phys. Rev. B - Condens. Matter Mater. Phys.*, 2012, **85**, 125136.